ACS APPLIED MATERIALS & INTERFACES

Research Article

www.acsami.org

Reversible Thermal Stiffening in Polymer Nanocomposites

Erkan Senses, Andrew Isherwood, and Pinar Akcora*

Department of Chemical Engineering and Materials Science, Stevens Institute of Technology, Hoboken, New Jersey 07030, United States

Supporting Information

ABSTRACT: Miscible polymer blends with different glass transition temperatures (T_g) are known to create confined interphases between glassy and mobile chains. Here, we show that nanoparticles adsorbed with a high-T_g polymer, poly(methyl methacrylate), and dispersed in a low-T_g matrix polymer, poly(ethylene oxide), exhibit a liquid-to-solid transition at temperatures above T_g's of both polymers. The mechanical adaptivity of nanocomposites to temperature underlies the existence of dynamically asymmetric bound layers on nanoparticles and more importantly reveals their impact on macroscopic mechanical response of composites. The unusual reversible stiffening behavior sets these materials apart from conventional polymer composites that soften upon heating. The presented stiffening mechanism in polymer nanocomposites can be used in applications for flexible electronics or mechanically induced actuators responding to environmental changes like temperature or magnetic fields.

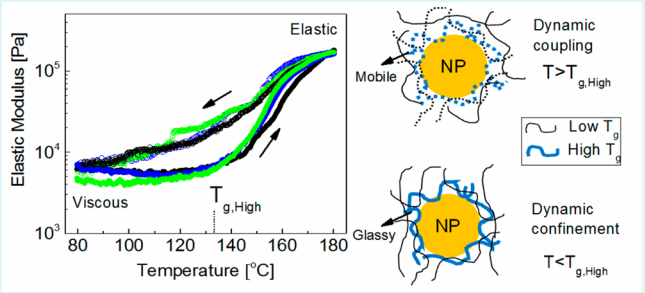

KEYWORDS: *polymer nanocomposite, miscible blend, dynamic coupling, confinement, reversible stiffening, interphase, adaptive*

INTRODUCTION

It is often desirable for materials to sustain fluidity at low temperature and exhibit reinforcement in the molten state. It is, however, a challenging task to retain mechanical performance, particularly in viscoelastic materials, with heating. This behavior, which holds a critical importance for mechanical adaptivity in soft materials, may be achieved with reversible stiffening at high temperatures. Reversibly stiffening nanocomposites can lead to transformative applications in soft robotics and flexible electronics where mechanical integrity should be maintained with internal heating in such systems.

Stiffening in soft materials has been realized through responsive polymers or reversible cross-linking mechanism.[1−4] For example, layered films of poly(*N*-isopropylacrylamide) (PNIPAM) tethered Au nanoparticles exhibit reversible hardening near the lower critical solution temperature (LCST) of PNIPAM, yet the moduli remain below kPa's because of solvent.[2] Dynamic supramolecular linkages[5,6] and thermoreversible cross-linking[7−9] yield reversibility in elastic properties of hydrogels and networks with remarkable self-healing character; however, these materials do not exhibit liquid-to-solid transition, as they are often permanently cross-linked. Carbon nanotube filled polydimethylsiloxane and liquid crystal elastomers under cyclic deformation are shown to self-stiffen,[10−12] yet these mechanisms either are irreversible or require structural changes such as crystal orientation and stress-activated chemical reactions. In this work, a new reversible thermal-stiffening mechanism in solvent-free polymer nanocomposites (PNCs) of polymer-adsorbed nanoparticles is demonstrated without using reversibly cross-linking or temperature responsive polymers.

It is well established that mechanical behavior of PNCs is controlled by matrix−filler interphases and dispersion,[13−15] which are both governed by ligand type on nanoparticles and polymer chemistry. In nanocomposites, interactions between physically adsorbed polymer layer on particles (i.e., extent of entanglements) and matrix chains determine the mechanical properties of PNCs.[16−18] We recently showed that entanglements of free chains with the bound layer can irreversibly grow under large periodic oscillatory shear.[19] In another work, particles adsorbed with poly(methyl methacrylate) chains of bimodal lengths (e.g., bimodal polymer bound layers) are used to reveal the effect of bound layer composition (chain dispersity) on mechanical properties.[17] The stability of long chains confirmed by IR analysis verified that adsorption of entangling chains is irreversible.[17] In this work, we exploit dynamic heterogeneity between adsorbed and free chains and explore its impact on macroscopic mechanical properties of bulk PNC films. Dynamically heterogeneous interphases contain polymers with large T_g differences and are used here to achieve reversible thermal-stiffening in polymer nanocomposites.

Dynamic asymmetry in miscible form (e.g. PEO−PMMA, PVME−PS, PVAc−PEO) has been studied in polymers that are rich in high-T_g component.[20−24] At sufficiently low temperatures, low-T_g polymer is confined within glassy chains. Consequently, low-T_g chains remain highly mobile as their dynamics is decoupled from surrounding chains. This effect is

Received: March 8, 2015
Accepted: June 17, 2015
Published: June 17, 2015

DOI: 10.1021/acsami.5b02046
ACS Appl. Mater. Interfaces 2015, 7, 14682−14689

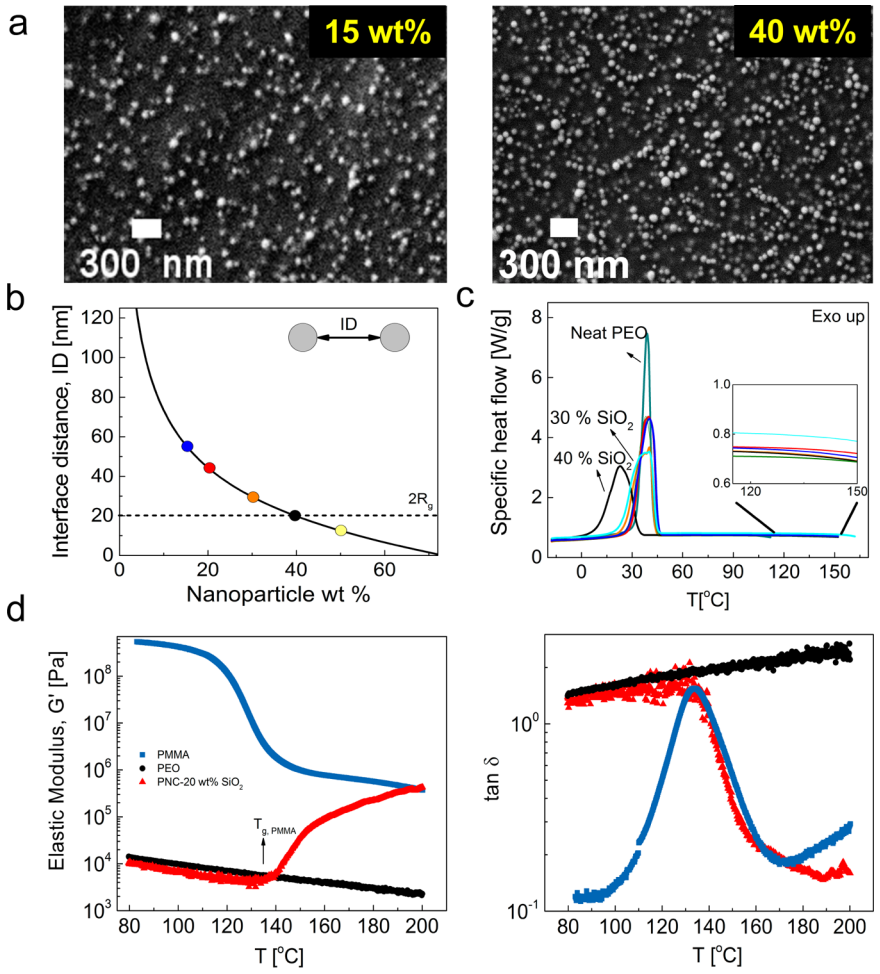

Figure 1. Sample characteristics and mechanical behavior of PMMA adsorbed SiO_2 nanoparticles in PEO matrix relative to pure polymers. (a) Scanning electron micrographs on freeze-fractured surfaces of nanocomposites with 15 and 40 wt % SiO_2 adsorbed with 68 kg/mol PMMA show well dispersion of nanoparticles in PEO matrix. (b) Average interparticle distance (ID) versus particle loading. Dashed line is for the matrix chain size ($2R_g$). (c) Melting temperatures of neat PEO and composites are obtained in heat flow curves. (d) Elastic modulus, G', behavior of PMMA, PEO, and 20 wt % composite versus temperature (at 5 °C/min heating rate) and their corresponding loss tangent behavior.

called dynamic confinement, since chain segments of the high T_g polymer are considered static on the time scale of segmental motions of the low-T_g component. At higher temperatures, however, both chains are mobile with different but cooperative relaxation times.[25] Such dynamic heterogeneity is commonly attributed to compositional heterogeneities due to thermal fluctuations[26] or self-concentration due to chain connectivity.[27] By adsorbing a high-T_g polymer (PMMA) on 55 nm silica nanoparticles and uniformly dispersing them in a low-T_g matrix (PEO), we aim to tune the mechanical response of composites with an effective interphase layer that becomes more mobile due to dynamic confinement of PEO chains within glassy PMMA at temperatures below $T_{g,PMMA}$. Here, we present the unique mechanical behavior of PEO composites and the effect of dynamic asymmetry near particle interphases on thermo-stiffening response.

EXPERIMENTAL SECTION

Materials. PMMA at different molecular weights were synthesized by ATRP polymerization using *p*-toluenesulfonyl chloride (TsCl) initiator, CuBr−$CuBr_2$ catalyst system with 2,2′-bipyridine in toluene under nitrogen environment at 70 °C. Colloidal SiO_2 nanoparticles (MEK-ST-L, 55 nm) dispersed in methyl ethyl ketone were supplied by Nissan Chemical America Corporation and used as received. PEO (−OH terminated and M_v = 100 000 g/mol) was purchased from Sigma-Aldrich and vacuum-dried for 3 days at room temperature.

Adsorbing Polymer on Nanoparticles. PMMA was dissolved in acetonitrile (at ∼30 mg/mL) before colloidal SiO_2 was added at 30 wt % and mixed in a bath sonicator for 30 min. Solution was stirred vigorously for 2 h. Particles adsorbed with PMMA were recollected by centrifugation at 11 000 rpm for 5 min. Washing process was repeated 3 times to ensure all unbound chains were removed. Finally, collected particles were dispersed at 4−6 wt % in acetonitrile. Dynamic light scattering measurements were carried out with a Zetasizer NanoS (Malvern Instruments) at particle concentration of ∼1 mg/mL in acetonitrile to measure the hydrodynamic thickness of adsorbed layers. Measurement duration was 11 s, and data were averaged over 10 runs. Thermal gravimetric analyzer measurements were performed on a Q50 TGA (TA Instruments) to determine the mass amount of adsorbed polymer on nanoparticles. Measurements were performed under a constant flow of nitrogen of 20 mL/min at a heating rate of 20 °C/min, starting from 40 °C up to 580 °C, while pausing isothermally at 150 °C for 20 min to ensure samples were free of solvent and then finally incubated at 580 °C for 20 min.

Nanocomposite Preparation and Characterization. PEO was dissolved in acetonitrile at 25 mg/mL, and PMMA bound particles were added while stirring polymer solution. Final solutions were stirred vigorously for 30 min and cast into Teflon dishes to form bulk films of ∼100−150 μm films. Films were then annealed at 90 °C for 2 d, at 120 °C for 12 h, and finally at 130 °C for 2 h under vacuum to

DOI: 10.1021/acsami.5b02046
ACS Appl. Mater. Interfaces 2015, 7, 14682−14689

remove any residual solvent. SEM images were obtained using a Zeiss Auriga dual-beam FIB-SEM instrument on freeze-fractured surfaces of the films. DSC was used to measure T_g and crystallization temperature. To determine T_g, 5−10 mg samples were first heated to 175 °C for 5 min and then cooled to 30 °C at 20 °C/min cooling rate followed by a heating ramp to 175 °C by 10 °C/min heating rate. T_g's were determined from the inflection point on heating curves. For melting temperature, samples were first equilibrated at −70 °C and then heated to 170 °C at 20 °C/min. After isothermal waiting for 5 min, samples were cooled back to −70 °C at the same rate. This cycle was repeated, and crystallization temperatures were determined from the second cooling curves.

Rheological Characterization. Rheology experiments were performed on a strain-controlled ARES-G2 (TA Instruments) with 8 mm stainless-steel parallel plate fixtures in a forced convection oven maintaining temperature within ±0.1 °C in nitrogen. Samples were molded with a vacuum assisted compression molder at 90 °C. For temperature sweep experiments, samples were first heated to 190 °C and thermally equilibrated to ensure complete melting and then cooled to 85 °C at 5 °C/min and equilibrated for 5 min. Temperature sweep experiments were performed at a strain amplitude of 0.5% (in linear regime for the whole temperature range) and at 5 rad/s with 5 °C/min heating rate. Modulus data were collected at 0.2 Hz sampling rate. Heating−cooling cycle scans were performed following the same protocol. Isothermal aging response was determined by pausing the heating and cooling scans at desired temperatures, and modulus data were collected. Measurements were done in quasi-equilibrium at which rate of deformation was much faster than the heating rate. This was confirmed on neat polymers with isothermal responses followed by heating steps shown in Figure S8d,e, Supporting Information. Strain amplitudes in linear regions at different temperatures for each frequency are determined. Creep-recovery tests were performed at different temperatures following 10 min equilibration. Small constant stress of 100 Pa was applied and deformation was monitored for 5 min, and then stress is decreased to zero to monitor the recovery. For temperature response of neat PMMA, samples were heated to 200 °C and waited for 10 min and then cooled to 110 °C at 10 °C/min rate and waited for 10 min for thermal equilibrium. Samples were then heated to 200 °C at 5 °C/min while small strain amplitude of 0.1% is applied at 5 rad/s frequency with data collected at 0.4 Hz. Data below 110 °C were obtained similarly but at high-torque mode of the instrument to prevent overshoot.

Small-Angle X-ray Scattering (SAXS). Measurements were performed at the beamline 8-ID-I in Advanced Photon Source at Argonne National Laboratory. The sample volume of 20 μm × 20 μm × 1000 μm was illuminated by coherent X-rays of 11 keV photon energy. SAXS pattern over the wave vector range 0.027 $nm^{-1} < q < 0.3$ nm^{-1} was obtained at 75, 90, 120, 140, and 160 °C with 10 min thermal equilibration priori. SAXS patterns were collected at five different locations on samples to evaluate uniformity and stability of the particle dispersion and distribution at different temperatures.

RESULTS AND DISCUSSION

We first adsorbed PMMA of different chain lengths (68 and 2.3 kg/mol) on 55 nm colloidal silica (SiO_2) nanoparticles and then mixed them with PEO matrix (M_w = 100 kg/mol). Figure 1a shows that nanoparticles are well dispersed in PEO at different particle concentrations (15 and 40 wt %). Confinement of chains is controlled with particle loading, which occurs typically at distances where interparticle distance (ID) is smaller than $2R_g$ of the polymer. Figure 1b presents that confinement factor becomes obvious at 50 wt % composition where ID becomes smaller than $2R_g$. ID is calculated using the equation $ID = d((\phi_{max}/\phi)^{1/3} - 1)$. d is the number-average particle diameter. ϕ_{max} is the maximum volume packing fraction which is $2/\pi$ for randomly distributed particles, and ϕ is the volume fraction of particles. We note that confinement of chains does not play a role in the mechanical behavior of composites discussed in this work, as particle compositions are lower than 50 wt %. Bulk T_g for 68 and 2.3 kg/mol PMMA is determined to be 130 and 92 °C, respectively, using a differential scanning calorimetry (DSC) instrument (Figure S1, Supporting Information). PEO−PMMA is an LCST type blend system[28,29] and has been shown to be miscible above 230 °C for similar molecular weights.[30] We chose our experimental temperature range to be 80−200 °C above the crystallization temperature of nanocomposites (Figure 1c). Note that T_g of PMMA and PEO is 135 and −65 °C, respectively. The amount of adsorbed PMMA is very small at ∼8 wt %, even in the highest particle loading of 50 wt %, and its T_g could not be measured in DSC for nanocomposites.

Thermal history of the samples and thermal equilibriumare important for rheology experiments. Figure S2, Supporting Information, shows the time evolution of linear elastic moduli of neat homopolymer PMMA and PEO; and PEO composites with 30 wt % PMMA bound SiO_2 nanoparticles at different temperatures. Samples were heated to a desired temperature with 5 °C/min heating rate, and data are collected immediately after the set temperature is reached. At 180 °C, moduli increase slightly with time. Note that moduli remains unchanged for the neat polymers. Temperature sweep experiments start at 85 °C, where there is no time dependence of moduli in any sample (see Figure S2). The same heating/cooling protocol was used for all samples to eliminate any possible thermal history effect on our mechanical results. For frequency and temperature sweep experiments, 5 min of equilibration time was applied at all temperatures.

Dynamic linear mechanical response (at fixed frequency, 5 rad/s) for homopolymers and 20 wt % composite with PMMA (68 kg/mol, Đ = 1.13) adsorbed SiO_2 particles to a temperature ramp (5 °C/min) is presented in Figure 1d. Bulk PMMA undergoes a glass−rubber transition at ∼135 °C as also seen in the loss tangent peak. Neat PEO behaves as a viscous liquid with low elastic moduli (∼kPa) decreasing monotonically with temperature. The composite behaves similarly to PEO up to $T_{g,PMMA}$ with typical moduli below 10 kPa and then stiffens with temperature beyond $T_{g,PMMA}$ to a modulus close to the entanglement plateau of PMMA (1.8 MPa). Loss tangent (ratio of viscous modulus to elastic modulus) for the composite clearly shows transition from liquid-to-solid states with temperature. At temperatures lower than T_g of PMMA, PEO matrix chains are dynamically decoupled, as they are highly mobile within glassy PMMA chains. The frozen PMMA chains do not contribute to composite relaxation; thus, matrix PEO chains govern the flow behavior. At temperatures higher than T_g of PMMA, ($T_{g,Matrix} < T_{g,Adsorbed} < T$), both matrix and adsorbed chains are mobile; hence, PEO chains are highly entangled with the mobile and pinned PMMA chains. These entangled chains yield stronger interfacial resistance than the pure bulk PEO. The slow dynamics of the high-T_g adsorbed chains leads to slowing of the PEO chain dynamics at the interphase due to highly entangled chains. This proposed mechanism is illustrated in Scheme 1. In a recent work, Richter et al.[16] showed that the mobile bound polymer chains form an effective interphase region where the full chain relaxation is impeded through the interaction with the anchored chains. We suggest that similar topological interactions arise in our system from the mixing of PEO and pinned PMMA segments between particle−polymer interphases. Therefore, slow motions of chains at the interphase give rise to a controlled stiffening in the low-T_g matrix. Note that the modulus of PEO

DOI: 10.1021/acsami.5b02046
ACS Appl. Mater. Interfaces 2015, 7, 14682−14689

Scheme 1. Schematic Illustration of Thermoresponsive Interphases in a Polymer Nanocomposite[a]

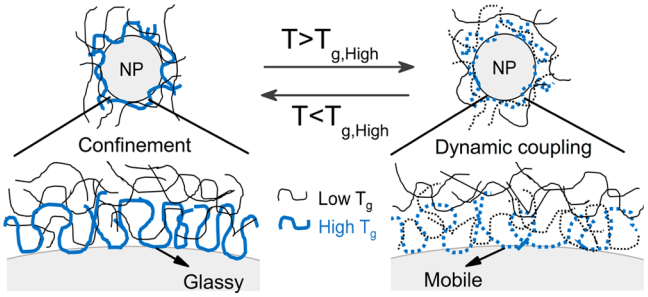

[a]Nanoparticles adsorbed with PMMA (thick blue lines) are dispersed in a miscible polymer PEO matrix (thin black lines). At temperatures below T_g of PMMA, as shown on the left, PEO chains are confined within frozen PMMA loops and dynamically decouple from polymer on surface. At temperatures higher than T_g of PMMA, as shown on the right, adsorbed polymer becomes mobile and dynamically couple with matrix chains. This dynamic coupling between two miscible polymers on particle interphases slows the dynamics of PEO and hence stiffens the matrix polymer at temperatures higher than T_g's of both polymers.

homopolymer is higher than its composite at temperatures below $T_{g,PMMA}$. This is due to the dynamic confinement as previously mentioned in the Introduction that PEO chains become highly mobile near nanoparticles due to confinement of PEO within glassy PMMA chains which results in reduced composite modulus.

By increasing the particle loading, liquid-to-solid transitions broaden as shown in Figures 2a,b. At low loadings (15 and 20 wt %), lower extent of stiffening is observed. The shift in transition temperature for these loadings may be due to the higher mobility needed to enable dynamic loops that will entangle with PEO. Additionally, loss angle behavior presents a liquid-to-rubbery transition for all compositions. It is seen in Figure 2a that the modulus of PEO/PMMA blend with 95:5 wt/wt composition decreases with temperature similar to neat PEO, which indicates that stiffening arises from nanoparticles adsorbed with long polymer chains. Molecular weight of adsorbed polymer also affects the thermostiffening because shorter chains have lower T_g's due to entropic contribution of chain ends and loop formations; hence, their interfacial entanglements are negligible compared to long chains. Particles adsorbed with short PMMA chains as shown in green data (2.3 kg/mol; Đ = 1.13) do not effectively stiffen the composites compared to other samples with 68 kg/mol PMMA adsorbed particles.

To verify the effect of dynamic coupling between PEO and PMMA on particle interphases, we prepared PEO composites with bare SiO_2 particles. Figure 2c and Figure 2d show that elastic moduli of PEO−SiO_2 composites soften with temperature and they are reinforced with increasing particle loadings. At high temperatures, bound and matrix chains soften in melt state. Frequency sweep data (Figure S3, Supporting Information) display a typical reinforcement with low-frequency plateau at high loadings. Thus, temperature and frequency sweeps on

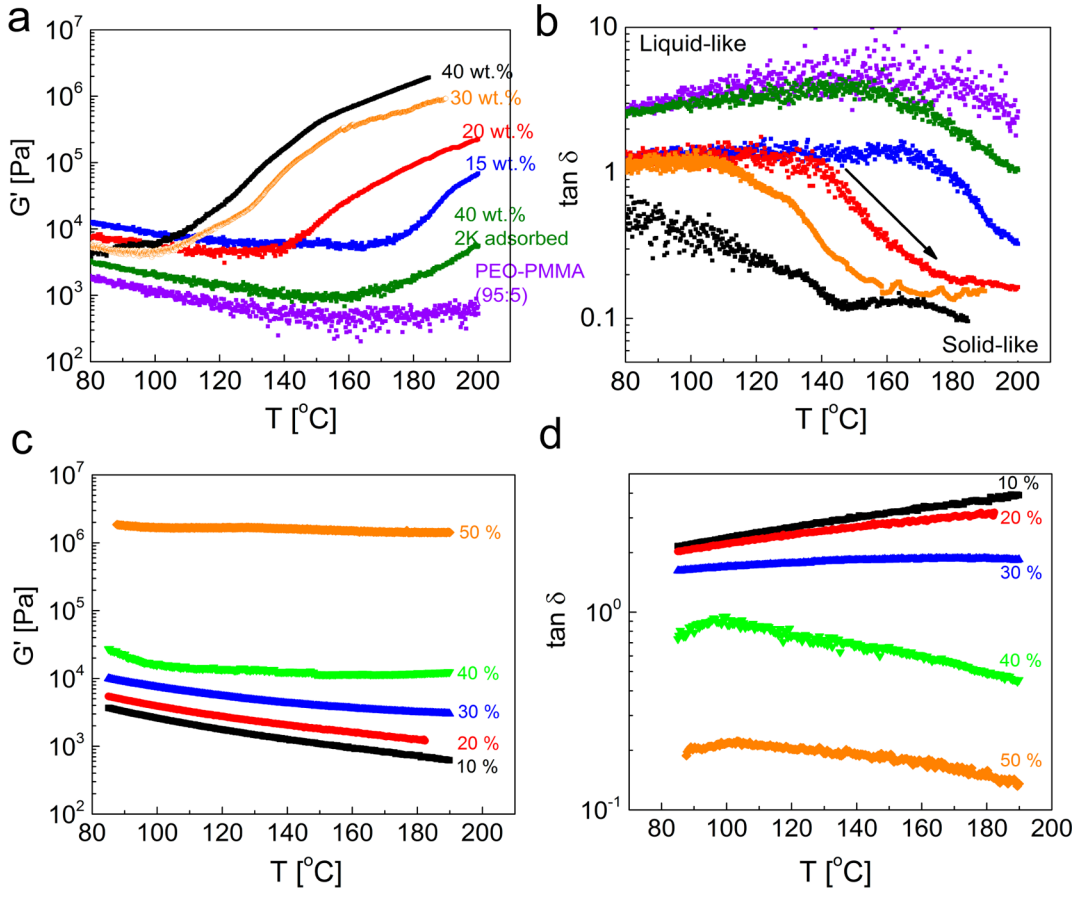

Figure 2. Effect of particle loading on mechanical response of nanocomposites. (a) Elastic moduli and (b) loss tangents of 68 kg/mol PMMA adsorbed particles in PEO with various particle loadings. (c) Elastic moduli and (d) loss tangents of PEO−bare SiO_2 particles.

DOI: 10.1021/acsami.5b02046
ACS Appl. Mater. Interfaces 2015, 7, 14682−14689

PEO−SiO_2 samples verify the importance of a high T_g bound chains on mechanical properties.

Dispersion stability at different temperatures was checked by running the composites in small-angle X-ray scattering experiments. Figure S4 in Supporting Information shows that particle dispersion does not change with temperature in both PEO−SiO_2 and PMMA-adsorbed SiO_2 in matrix PEO.

We further tested the chain length effect by adsorbing long PMMA chains (M_w = 200 kg/mol, Đ = 1.17) (Figure 3) and

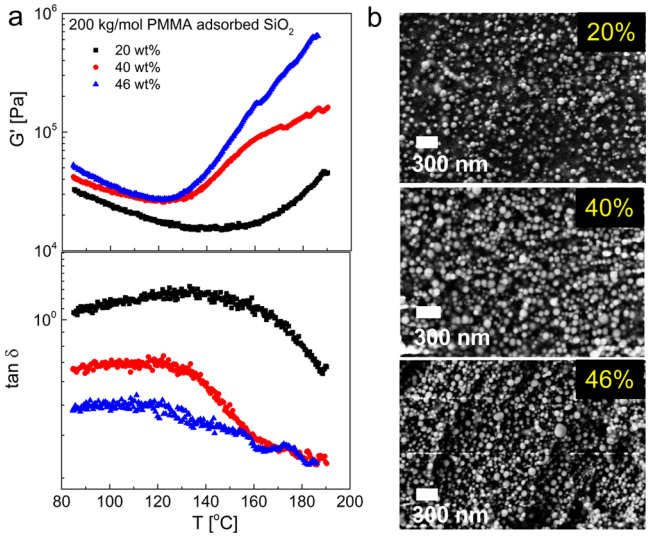

Figure 3. Stiffening response from longer adsorbed chains. (a) Elastic moduli and loss tangents of composites with 200 kg/mol PMMA (Đ = 1.17) adsorbed SiO_2 with increasing temperature. (b) Dispersions at 20, 40, and 46 wt % are shown in SEM images.

short PMMA chains (M_w = 9.6 kg/mol, Đ = 1.06) (Figure S5, Supporting Information). Particles adsorbed with longer chains reinforce the composites at low temperatures and exhibit thermostiffening at elevated temperatures. Composites of 10 kg/mol PMMA adsorbed particles behave similar to bare SiO_2 composites and soften by heating at 10, 20, and 30 wt % loadings. We observed an increase in modulus only at the highest loading (40 wt %) that reaches a high temperature plateau which is not seen in other composites. Also note that 40 wt % composite has smaller low-temperature modulus compared to 30 wt % loading, which is similar to the low-temperature modulus trend shown in Figure 2a. The low temperature response of composites again indicates that dynamic confinement enhances the mobility.

Deformation rate also has a strong effect on thermostiffening. Frequency sweeps of a 30 wt % composite (Figure 4a,b) present unusually high modulus at higher temperatures with no frequency dependence which is a typical elastic network response. Since at high frequency, relaxation time of PMMA is greater than the applied deformation rate, it is still glassy and the relaxation is governed by PEO chains whose dynamics is not very much affected. However, at lower frequencies, even at the same temperature, PMMA relaxation rate becomes comparable to deformation rate; thus, the dynamic coupling occurs between two mobile chains with different relaxation rates. The result is the increase of moduli at low frequencies. Upturns at low frequencies above $T_{g,PMMA}$ suggest aging of the sample between long deformation cycle times. Note that this increase does not occur at $T < T_{g,PMMA}$, suggesting that the relaxation rate of PMMA is out of the experimental deformation rate, so it behaves glassy for the whole range of frequencies. At higher temperatures PMMA is mobile; thus, it behaves elastic at any frequency.

We applied a temperature ramp with fixed 1, 5, and 50 rad/s deformation frequencies (Figure 4d) to evaluate the effect of deformation rate. At high temperatures, moduli become independent of frequency, while low-temperature moduli increase with frequency, which is in line with frequency sweep results. It is noteworthy that the transition temperature shifts from 130 to 150 °C with frequency because of insufficient time for relaxation to occur at high frequencies, which in turn shifts T_g to higher temperatures. Flow and deformability of a 30 wt % composite were further tested at a constant stress of 100 Pa (creep) and subsequent recovery in cessation (Figure 4c). At 110 °C, polymer is viscoelastic and steadily flows with time; however, at high temperatures (170 and 190 °C), deformability decreases and strain remains constant over time.

Periodic temperature scans (at 5 °C/min) of a 40 wt % sample between 80 and 180 °C show that stiffening/softening is achieved over many cycles (Figure 5a,b). Complex viscosity presents similar increase by heating and completely reverts to its original value upon cooling, with clear thermal hysteresis centered around $T_{g,PMMA}$. It is demonstrated in Figure 5c that the composite and neat PEO flow at 120 °C and composite retains its bulk shape at 190 °C compared to PEO melt. Increase in elastic modulus with temperature is linear above transition temperature with a typical slope of ∼4.8 kPa/°C ± 1.2 (Figure S6, Supporting Information). Since mechanical behavior is governed by the coupling of fast PEO and slow PMMA dynamics within interphases at high temperatures, the slowing dynamics of PEO causes stiffening mechanism that is analogous to network elasticity. Modulus of a polymer network increases linearly with temperature and can be approximated by $G = \rho RT/M$ in a small deformation regime. Since bulk density of PEO[31] is 1.06 g/cm and the entanglement molecular weight M is 1730 g/mol, slope of the modulus of an entangled polymer network is calculated as 5 kPa/°C, which is equal to the slope of the stiffening obtained in our experiments (Figure S6).

Bound and matrix chains are chosen to be chemically identical in most polymer nanocomposites. The mechanical reinforcement in various composite systems was explained with the bound layer and interphase effects.[32−36] In previous work, we showed that interactions between polymer-graft chains control the mechanical reinforcement.[33] It is also shown that percolating particle−polymer network is essential where particles serve as network junctions.[34] Here, we present a different perspective to the reinforcement mechanism that composites are reinforced when bound chains are mobile. This result is consistent with the findings of Richter's work which showed that chain relaxations slow down by the anchored chains.[16]

Time evolution of elastic moduli demonstrates aging of composites above T_g of PMMA. We interrupted heating and cooling cycles with isothermal steps (Figure 6a and Figure S7, Supporting Information) and measured the growth rates of elastic moduli for 68 kg/mol PMMA adsorbed SiO_2 (Figure 6b). Changes in the moduli during cooling steps show that stiffening is both temperature and time dependent. The modulus spikes during resting time and drops again in cooling, which is seen at temperatures above $T_{g,PMMA}$ as stiffening continues when bound chains are mobile. This behavior

DOI: 10.1021/acsami.5b02046
ACS Appl. Mater. Interfaces 2015, 7, 14682−14689

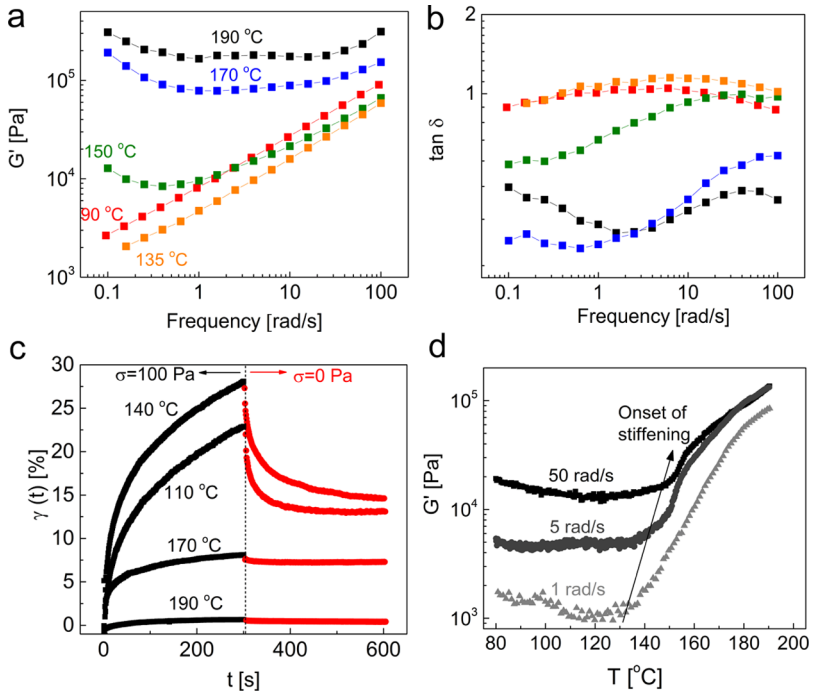

Figure 4. Frequency dependence of thermostiffening and creep-recovery behavior. Effect of linear deformation frequency on (a) elastic modulus and (b) loss tangent at different temperatures of a 30 wt % composite displays frequency-independent moduli at low temperature while presenting unusually high elastic moduli at high temperatures. Upturns at low frequencies imply aging response between two data points. (c) Strain response of the same composite to a constant stress of 100 Pa (creep) and corresponding recovery upon removal of stress at different temperatures. (d) Temperature sweeps (5 °C/min) at different linear deformation frequency show the onset of stiffening is shifted to higher temperatures with frequency.

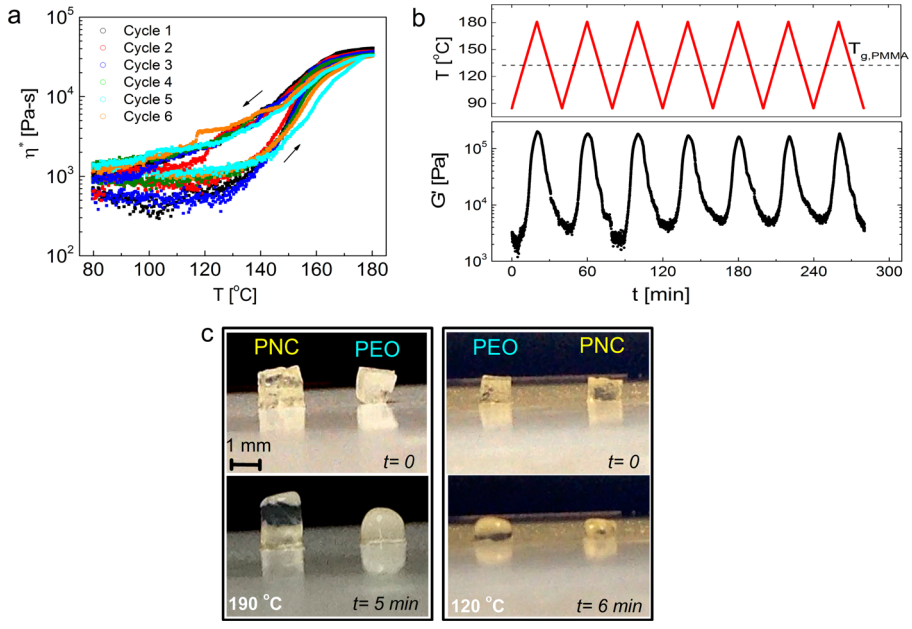

Figure 5. Reversibility in complex viscosity and elastic moduli. (a) Complex viscosity behavior of a 40 wt % composite upon heating and cooling cycles (5 °C/min) follows the same heating and cooling paths with hysteresis around $T_{g,PMMA}$. (b) Elastic modulus of a 40 wt % composite in response to periodic temperature scans between 80 and 180 °C. (c) PEO and 30 wt % composite (PNC) show similar deformability after waiting for 6 min at 120 °C. At higher temperatures (190 °C), PEO melts and PNC retains its shape.

indicates the quick dynamic stiffening response of the composites during resting. At 80 °C, the spike gets smaller, since PMMA gets glassy and PEO becomes more mobile. The slow evolution of modulus during resting time is indicative of a network-like behavior of composites where entanglements evolve slowly.

Note that stiffening rates in the composite are similar in heating and cooling steps. We applied the same protocol on neat PMMA and PEO and observed that both polymers soften with heating (Figure S8, Supporting Information). This verifies that high temperature aging is not due to thermal equilibration of neat components. All composites showed Arrhenius-type

DOI: 10.1021/acsami.5b02046
ACS Appl. Mater. Interfaces 2015, 7, 14682−14689

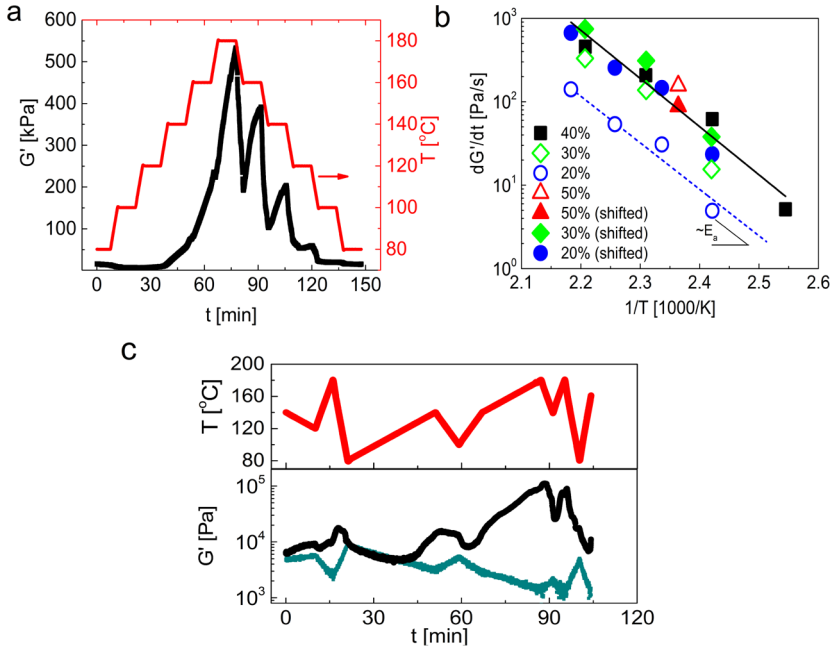

Figure 6. Aging dynamics and thermal stiffening of nanocomposites. (a) Stepwise temperature increment (with 5 °C/min heating rates) on a 30 wt % nanocomposite reveals that stiffening rate is temperature dependent and reversible upon cooling. (b) Stiffening rates for different compositions follow an Arrhenius behavior. Activation energy, which is the slope of the fitted lines, is 108 kJ/mol at different particle concentrations. (c) Mechanical response of neat PEO (green line) and 30 wt % nanocomposite (black line) to an arbitrary thermal load applied between 80 and 180 °C with 2−20 °C/min temperature ramps.

dependence on stiffening rates (Figure 6b), with the same activation energy of $E_a \approx 108$ kJ/mol. The vertical shift of the curves for composites with larger interparticle separation is presumably because of the larger diffusion distances for interfacial effect to propagate into bulk matrix. We obtain the stiffening rate response for equivalent diffusion distance in each composite by shifting the kinetic data vertically by a factor of $[ID/(2R_g)]^2$. The points overlap on a linear line, suggesting that the mechanism for aging is independent of particle loading, yet slower for large interparticle separations.

Finally, we demonstrate the performance of a 30 wt % thermostiffening composite to an arbitrary temperature change between 80 and 180 °C, subjected to different ramps at 2−20 °C/min (Figure 6c). It is seen that while PEO softens with temperature, PNC follows the thermal trace and stiffens with increasing temperature. Aging response becomes more apparent at slow heat ramps, whereas at fast ramps composites can also thermally stiffen.

CONCLUSIONS

Our results demonstrate that confinement and coupling mechanism of dynamically asymmetric polymer blends with nanoparticles enable self-stiffening in solvent-free nanocomposites. The mechanism presented here is driven by large T_g disparity of polymers at interphases and controlled by mobility of the high-T_g bound polymer layer on nanoparticles. When bound layer is frozen, PEO behaves more mobile within glassy regions than pure PEO; on the contrary, at high temperatures the highly mobile adsorbed chains enable entanglements between anchored and matrix chains and are responsible for transmitting the surface dynamics into the bulk of the polymer. From the temperature dependent mechanical relaxation in our system, we conclude that the mobility of adsorbed chains is essential for reinforcement. Consequently, an unusual and thermoreversible liquid-to-elastic transition can be achieved in melt systems. We conjecture that similar thermostiffening may be achieved in polymers loaded with functional fillers such as magnetic and plasmonic nanoparticles to design shape changing and stiffening materials, which can lead to their transformative applications in soft robotics and flexible electronics.

ASSOCIATED CONTENT

Supporting Information

Dynamic light scattering data and thermal characterization of homopolymers and polymer adsorbed particles; time evolution of linear elastic moduli of neat PMMA, PEO homopolymers, and PEO composites; SAXS data of composites containing bare and PMMA adsorbed nanoparticles; linear viscoelastic data of PEO−SiO_2 nanocomposites at 0−50 wt % filler loadings; stiffening response from short adsorbed chains; elastic modulus−temperature profiles of 40 and 50 wt % composites; chain length effect on isothermal stiffening; growth rate of elastic moduli to stepwise temperature changes. The Supporting Information is available free of charge on the ACS Publications website at DOI: 10.1021/acsami.5b02046.

AUTHOR INFORMATION

Corresponding Author

*E-mail: pakcora@stevens.edu.

Notes

The authors declare no competing financial interest.

ACKNOWLEDGMENTS

We acknowledge financial support from Stevens start-up funds and partial funding from NSF-DMR CAREER (Grant 1048865). This research used resources of the Advanced Photon Source, a U.S. Department of Energy (DOE) Office of Science User Facility operated for the DOE Office of Science

DOI: 10.1021/acsami.5b02046
ACS Appl. Mater. Interfaces 2015, 7, 14682−14689

by Argonne National Laboratory under Contract DE-AC02-06CH11357. SAXS data were collected at the 8-ID-I beamline at the Advanced Photon Source, Argonne National Laboratory.

REFERENCES

(1) Hu, Z.; Xia, X. Hydrogel Nanoparticle Dispersions with Inverse Thermoreversible Gelation. *Adv. Mater.* **2004**, *16*, 305−309.
(2) Zhu, Z.; Senses, E.; Akcora, P.; Sukhishvili, S. A. Programmable Light-Controlled Shape Changes in Layered Polymer Nanocomposites. *ACS Nano* **2012**, *6*, 3152−3162.
(3) McKee, J. R.; Hietala, S.; Seitsonen, J.; Laine, J.; Kontturi, E.; Ikkala, O. Thermoresponsive Nanocellulose Hydrogels with Tunable Mechanical Properties. *ACS Macro Lett.* **2014**, *3*, 266−270.
(4) Ding, F.; Tang, Z.; Ding, B.; Xiong, Y.; Cai, J.; Deng, H.; Du, Y.; Shi, X. Tunable Thermosensitive Behavior of Multiple Responsive Chitin. *J. Mater. Chem. B* **2014**, *2*, 3050−3056.
(5) Chen, Y.; Kushner, A. M.; Williams, G. A.; Guan, Z. Multiphase Design of Autonomic Self-Healing Thermoplastic Elastomers. *Nat. Chem.* **2012**, *4*, 467−472.
(6) Montarnal, D.; Tournilhac, F.; Hidalgo, M.; Couturier, J.-L.; Leibler, L. Versatile One-Pot Synthesis of Supramolecular Plastics and Self-Healing Rubbers. *J. Am. Chem. Soc.* **2009**, *131*, 7966−7967.
(7) Chen, X.; Wudl, F.; Mal, A. K.; Shen, H.; Nutt, S. R. New Thermally Remendable Highly Cross-Linked Polymeric Materials. *Macromolecules* **2003**, *36*, 1802−1807.
(8) Zhang, Y.; Broekhuis, A. A.; Picchioni, F. Thermally Self-Healing Polymeric Materials: The Next Step to Recycling Thermoset Polymers? *Macromolecules* **2009**, *42*, 1906−1912.
(9) Lott, J. R.; McAllister, J. W.; Arvidson, S. A.; Bates, F. S.; Lodge, T. P. Fibrillar Structure of Methylcellulose Hydrogels. *Biomacromolecules* **2013**, *14*, 2484−2488.
(10) Carey, B. J.; Patra, P. K.; Ci, L.; Silva, G. G.; Ajayan, P. M. Observation of Dynamic Strain Hardening in Polymer Nanocomposites. *ACS Nano* **2011**, *5*, 2715−2722.
(11) Ramirez, A. L. B.; Kean, Z. S.; Orlicki, J. A.; Champhekar, M.; Elsakr, S. M.; Krause, W. E.; Craig, S. L. Mechanochemical Strengthening of a Synthetic Polymer in Response to Typically Destructive Shear Forces. *Nat. Chem.* **2013**, *5*, 757−761.
(12) Agrawal, A.; Chipara, A. C.; Shamoo, Y.; Patra, P. K.; Carey, B. J.; Ajayan, P. M.; Chapman, W. G.; Verduzco, R. Dynamic Self-Stiffening in Liquid Crystal Elastomers. *Nat. Commun.* **2013**, *4*, 1739.
(13) Bréchet, Y.; Cavaille, J.-Y.; Chabert, E.; Chazeau, L.; Dendievel, R.; Flandin, L.; Gauthier, C. Polymer Based Nanocomposites: Effect of Filler-Filler and Filler-Matrix Interactions. *Adv. Eng. Mater.* **2001**, *3*, 571.
(14) Chevigny, C.; Dalmas, F.; Di Cola, E.; Gigmes, D.; Bertin, D.; Boué, F. o.; Jestin, J. Polymer-Grafted-Nanoparticles Nanocomposites: Dispersion, Grafted Chain Conformation, and Rheological Behavior. *Macromolecules* **2011**, *44*, 122−133.
(15) Akcora, P.; Kumar, S. K.; García Sakai, V.; Li, Y.; Benicewicz, B. C.; Schadler, L. S. Segmental Dynamics in Pmma-Grafted Nanoparticle Composites. *Macromolecules* **2010**, *43*, 8275−8281.
(16) Krutyeva, M.; Wischnewski, A.; Monkenbusch, M.; Willner, L.; Maiz, J.; Mijangos, C.; Arbe, A.; Colmenero, J.; Radulescu, A.; Holderer, O.; Ohl, M.; Richter, D. Effect of Nanoconfinement on Polymer Dynamics: Surface Layers and Interphases. *Phys. Rev. Lett.* **2013**, *110*, 108303.
(17) Senses, E.; Akcora, P. Tuning Mechanical Properties of Nanocomposites with Bimodal Polymer Bound Layers. *RSC Adv.* **2014**, *4*, 49628−49634.
(18) Scheutjens, J.; Fleer, G. Statistical Theory of the Adsorption of Interacting Chain Molecules. 2. Train, Loop, and Tail Size Distribution. *J. Phys. Chem.* **1980**, *84*, 178−190.
(19) Senses, E.; Akcora, P. An Interface-Driven Stiffening Mechanism in Polymer Nanocomposites. *Macromolecules* **2013**, *46*, 1868−1874.
(20) Haley, J. C.; Lodge, T. P. Dynamics of a Poly (Ethylene Oxide) Tracer in a Poly (Methyl Methacrylate) Matrix: Remarkable Decoupling of Local and Global Motions. *J. Chem. Phys.* **2005**, *122*, 234914.
(21) Tyagi, M.; Arbe, A.; Alegria, A.; Colmenero, J.; Frick, B. Dynamic Confinement Effects in Polymer Blends. A Quasielastic Neutron Scattering Study of the Slow Component in the Blend Poly (Vinyl Acetate)/Poly (Ethylene Oxide). *Macromolecules* **2007**, *40*, 4568−4577.
(22) Tyagi, M.; Arbe, A.; Colmenero, J.; Frick, B.; Stewart, J. Dynamic Confinement Effects in Polymer Blends. A Quasielastic Neutron Scattering Study of the Dynamics of Poly (Ethylene Oxide) in a Blend with Poly (Vinyl Acetate). *Macromolecules* **2006**, *39*, 3007−3018.
(23) Lutz, T.; He, Y.; Ediger, M.; Cao, H.; Lin, G.; Jones, A. A. Rapid Poly (Ethylene Oxide) Segmental Dynamics in Blends with Poly (Methyl Methacrylate). *Macromolecules* **2003**, *36*, 1724−1730.
(24) Niedzwiedz, K.; Wischnewski, A.; Monkenbusch, M.; Richter, D.; Genix, A.-C.; Arbe, A.; Colmenero, J.; Strauch, M.; Straube, E. Polymer Chain Dynamics in a Random Environment: Heterogeneous Mobilities. *Phys. Rev. Lett.* **2007**, *98*, 168301.
(25) Ngai, K.; Roland, C. Unusual Component Dynamics in Poly (Ethylene Oxide)/Poly (Methyl Methacrylate) Blends As Probed by Deuterium NMR. *Macromolecules* **2004**, *37*, 2817−2822.
(26) Kamath, S.; Colby, R. H.; Kumar, S. K.; Karatasos, K.; Floudas, G.; Fytas, G.; Roovers, J. E. Segmental Dynamics of Miscible Polymer Blends: Comparison of the Predictions of a Concentration Fluctuation Model to Experiment. *J. Chem. Phys.* **1999**, *111*, 6121−6128.
(27) Lodge, T. P.; McLeish, T. C. Self-Concentrations and Effective Glass Transition Temperatures in Polymer Blends. *Macromolecules* **2000**, *33*, 5278−5284.
(28) Schwahn, D.; Pipich, V.; Richter, D. Composition and Long-Range Density Fluctuations in PEO/PMMA Polymer Blends: A Result of Asymmetric Component Mobility. *Macromolecules* **2012**, *45*, 2035−2049.
(29) Pedemonte, E.; Polleri, V.; Turturro, A.; Cimmino, S.; Silvestre, C.; Martuscelli, E. Thermodynamics of Poly (Ethylene Oxide)-Poly (Methyl Methacrylate) Blends: Prediction of Miscibility Based on the Corresponding-States Theory. *Polymer* **1994**, *35*, 3278−3281.
(30) Fernandes, A.; Barlow, J.; Paul, D. Blends Containing Polymers of Epichlorohydrin and Ethylene Oxide. Part I: Polymethacrylates. *J. Appl. Polym. Sci.* **1986**, *32*, 5481−5508.
(31) Fetters, L.; Lohse, D.; Colby, R. Chain Dimensions and Entanglement Spacings. In *Physical Properties of Polymers Handbook*; Mark, J. E., Ed.; Springer Science: New York, 2007; Chapter 25, pp 447−454.
(32) Papon, A.; Montes, H.; Lequeux, F.; Oberdisse, J.; Saalwächter, K.; Guy, L. Solid Particles in an Elastomer Matrix: Impact of Colloid Dispersion and Polymer Mobility Modification on the Mechanical Properties. *Soft Matter* **2012**, *8*, 4090−4096.
(33) Akcora, P.; Kumar, S. K.; Moll, J.; Lewis, S.; Schadler, L. S.; Li, Y.; Benicewicz, B. C.; Sandy, A.; Narayanan, S.; Ilavsky, J.; Thiyagarajan, P.; Colby, R. H.; Douglas, J. F. "Gel-like" Mechanical Reinforcement in Polymer Nanocomposite Melts. *Macromolecules* **2010**, *43*, 1003−1010.
(34) Moll, J. F.; Akcora, P.; Rungta, A.; Gong, S.; Colby, R. H.; Benicewicz, B. C.; Kumar, S. K. Mechanical Reinforcement in Polymer Melts Filled with Polymer Grafted Nanoparticles. *Macromolecules* **2011**, *44*, 7473−7477.
(35) Chen, Q.; Gong, S.; Moll, J.; Zhao, D.; Kumar, S. K.; Colby, R. H. Mechanical Reinforcement of Polymer Nanocomposites from Percolation of a Nanoparticle Network. *ACS Macro Lett.* **2015**, *4*, 398−402.
(36) Zhu, A. J.; Sternstein, S. S. Nonlinear Viscoelasticity of Nanofilled Polymers: Interfaces, Chain Statistics and Properties Recovery Kinetics. *Compos. Sci. Technol.* **2003**, *63*, 1113−1126.

DOI: 10.1021/acsami.5b02046
ACS Appl. Mater. Interfaces 2015, 7, 14682−14689